

Article

Research on Deployment Process Dynamics and Vibration for Replaceable Interface Mast

Tongliang Liu ¹ , Jianmin Wen ^{2,*} and Ping Zhang ²¹ Rongcheng College, Harbin University of Science and Technology, Rongcheng 264300, China; tll@hrbust.edu.cn² School of Ocean Engineering, Harbin Institute of Technology, Weihai 264209, China; pingzhang2018@163.com

* Correspondence: wenjm@hit.edu.cn

Abstract: The mast of the rover is a device used to carry precision instruments such as cameras on the rover, and its performance directly affects the working quality of these devices. The replaceable interface mast can effectively solve the problems of a single structure and poor maintenance of ordinary masts, so we study the deployment process dynamics properties and vibration for replaceable interface mast. Firstly, we analyzed the spatial motion of the reconfigurable rigid body module by the absolute node coordinate method and the natural coordinate method, and established the dynamic equation of the interface, the reconfigurable module without external constraints. Then, we established a dynamic model of the mast system deployment process. We analyzed the dynamic behavior of the replaceable interface mast and studied and compared the differences in the deployment behavior of the replaceable interface mast under different system configurations, flexible interface geometric parameters, and different driving rules. Finally, we built a model of the mast system and experimentally analyzed the deployment process of the replaceable interface mast. Using numerical solution and experimental verification, we proved that the established dynamic model of the mast system can correctly analyze the deployment behavior dynamics of the replaceable interface mast, and the study can provide a reference for the design and behavior analysis of the mast system.

Keywords: replaceable interface mast; reconfigurable module; dynamic properties; vibration



Citation: Liu, T.; Wen, J.; Zhang, P. Research on Deployment Process Dynamics and Vibration for Replaceable Interface Mast. *Machines* **2024**, *12*, 243. <https://doi.org/10.3390/machines12040243>

Academic Editor: Carmine Maria Pappalardo

Received: 27 February 2024

Revised: 25 March 2024

Accepted: 1 April 2024

Published: 8 April 2024



Copyright: © 2024 by the authors. Licensee MDPI, Basel, Switzerland. This article is an open access article distributed under the terms and conditions of the Creative Commons Attribution (CC BY) license (<https://creativecommons.org/licenses/by/4.0/>).

1. Introduction

The interplanetary rover mast is the mounting and support platform for highly sophisticated equipment, such as navigation topography cameras and multispectral cameras on the rover [1]. In the space field, the research direction of modular spacecraft and on-orbit replacement has received a lot of attention for its high maintainability, so on-orbit replacement can be applied to the rover mast to extend its service time in orbit. One of the key technologies of the modular spacecraft is the fast docking between the modules [2–6]. Most of the studies have focused on the analysis of the dynamics of the docking mechanism during the docking process [7–9] but less on the influence of the docking mechanism on the dynamics of the completed system after the docking. Therefore, it is necessary to analyze the behavior of the mast end during deployment and to compare the dynamic behavior of the mast under different module configurations, different interface geometry parameters, and different deployment joint drive laws to provide a basis for the structural and drive design of the replaceable interface mast. Fewer studies exist on the dynamical orientation of rover masts. In 2008, Li, Gao, et al. [10] used Lagrangian equations combined with the Newton-Euler method to model the dynamics of the lunar rover mast during unfolding; however, the flexibility of the mast was not considered in the model developed. In 2015, Liu et al. [11] designed a new mast-locking mechanism and modeled the dynamics of each joint. The position error of the mast end and the repeatability accuracy were analyzed, but the vibration deformation of the mast was also not considered. In 2017, Bindi You and Pei-Bo Hao [12] investigated the nonlinear dynamics characteristics of the mast deployment

process of a laminated composite rover considering deformation and gave the effect of the change of the laminated material's own parameters on the mast dynamics performance but did not analyze the mast end dynamics performance influenced by the motion of the deployment joints. The above studies provide a reference for the kinematic analysis of the rigid body of the replaceable mast in this study, but the flexible body structure is also included in the replaceable mast system, so related research on flexible body kinematics needs to be introduced.

The study of spacecraft dynamics with flexible accessories, such as spaceborne antennas and space manipulators, can also provide a certain reference for the study in this paper [13–17]. The multi-body system is divided into a multi-rigid body system and a multi-flexible body system. The development of multi-rigid body dynamics theory has become mature today, and the multi-flexible body system is the majority in practical problems, and the theoretical method of multi-flexible body dynamics can be mainly divided into floating coordinate system method and absolute node coordinate method [18–21]. The replaceable interface mast dynamics system is a typical multibody system that includes both rigid and flexible bodies, and the modeling methods with natural coordinates [22,23] and the absolute nodal coordinate formulation [24–26] are suitable and effective due to their own advantages. To establish the dynamic model of a rigid-flexible multi-body system, it is necessary to describe the rigid body motion and the deformation motion of the flexible body separately [27–31]. In this paper, the dynamics model of the replaceable interface mast system will be established to analyze the end nonlinear behavior of the mast deployment process.

The remaining parts of the paper are presented as follows: In Section 2, the materials and methods we selected are introduced. In Section 3, the effect of nonlinear parameters on mast deployment is analyzed. In Section 4, the main conclusions are summarized.

2. Materials and Methods

In dealing with the replaceable interface mast, the reconfigurable modules within the mast are considered rigid bodies. As shown in Figure 1, two fixed points, p and q , and two unit vectors, u and v , are used to establish a natural coordinate system, x - y - z , on the rigid module.

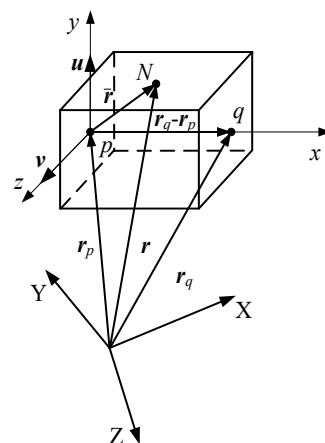


Figure 1. Description of the position of the rigid body module.

Let V_r represent the volume of the reconfigurable rigid body module, and ρ represent its density. The expression for the kinetic energy of the reconfigurable module can be calculated using Equation (1).

$$T = \frac{1}{2} \left(\int_{V_r} \rho (\mathbf{A}\dot{\mathbf{q}}_r)^T \mathbf{A}\dot{\mathbf{q}}_r dV_r \right) = \frac{1}{2} \dot{\mathbf{q}}_r^T \mathbf{M}\dot{\mathbf{q}}_r \quad (1)$$

where V_r is the Volume of reconfigurable modules, M is the quality matrix of the reconfigurable module, $M = \int_{V_r} \rho A^T A dV_r$; A is the shape functions of the rigid body module, q_r is a generalized coordinate system defined by the fixed point q , r is a position vector in the global coordinate system.

The virtual work of inertial forces for reconfigurable modules can be calculated by Equation (2).

$$\delta W_{gr} = - \int_{V_r} \rho \delta r^T \ddot{r} dV_r = - \delta q_r^T \left(\int_{V_r} \rho A^T A dV_r \right) \ddot{q}_r = - \delta q_r^T M \ddot{q}_r \quad (2)$$

The external virtual work of the reconfigurable module can be written as Equation (3).

$$\delta W_{er} = - \left(\delta q_r^T Q_F + \delta q_r^T Q_M \right) \quad (3)$$

In Equation (3), Q_F and Q_M , respectively represent the generalized force columns of external force and external moment in the natural coordinate system.

The virtual work performed by the force F acting at any point N on the rigid body module can be expressed as Equation (4).

$$\delta W_F = \delta r_N^T F = \delta q_r^T A_N^T F = \delta q_r^T Q_F \quad (4)$$

where A_N is the shape function corresponding to point N .

The virtual work of internal forces in the rigid body module is zero; hence, we can infer from the principle of virtual work as Equation (5).

$$- \delta q_r^T M \ddot{q}_r + \left(\delta q_r^T Q_F + \delta q_r^T Q_M \right) = - \delta q_r^T (M \ddot{q}_r - Q_F - Q_M) = 0 \quad (5)$$

where Q_F is the generalized force due to external forces, Q_M is the generalized force corresponding to the moment M .

Establish the intrinsic constraint equations for the reconfigurable module in the natural coordinate system as Equation (6).

$$\Phi(q_r, t) = 0 \quad (6)$$

The dynamic equations for the reconfigurable rigid body module in the absence of external constraints can be obtained in Equation (7).

$$\begin{cases} M \ddot{q}_r = Q_r \\ \Phi(q_r, t) = 0 \end{cases} \quad (7)$$

where $Q_r = Q_F + Q_M$.

The interface on the mast of the replaceable interface can be equivalently modeled as a cylindrical shell. The shell used in this paper has a thickness of $h = 2$ mm and a mid-surface radius of $R = 41$ mm. Thus, the interface can be represented by thin shell elements. The schematic diagram of the shell element deformation is shown in Figure 2.

The present study employs the gradient-reduced ANCF (Absolute Nodal Coordinate Formulation) thin shell element [21,28] to discretize the finite element of the flexible interface's equivalent cylindrical shell model. The deformation along the thickness of the thin shell is neglected, and the overall deformation of the shell element is described using the stretching and shearing deformations on the mid-surface of the cylindrical shell element, as well as the bending deformation of the element.

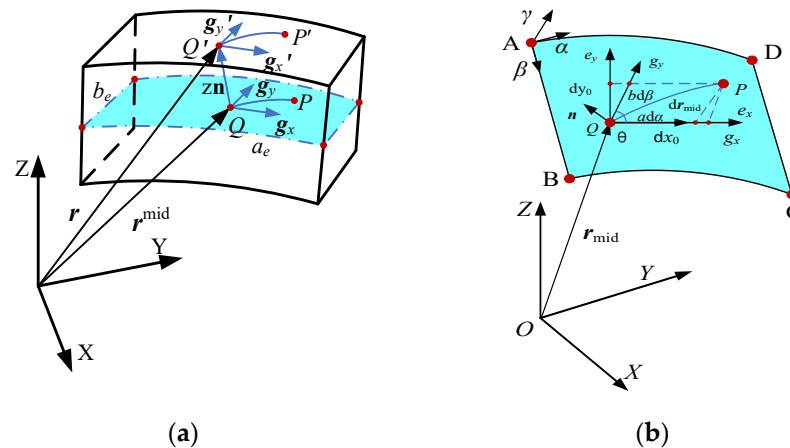


Figure 2. The schematic diagram of the shell element deformation. (a) shell unit deformation, (b) the middle surface of the shell unit.

2.1. Description of the Movement of the Shell Unit

The nodal coordinates of the shell element, denoted as “e”, are composed of the position coordinates and gradient coordinates of four points A, B, C, and D on the neutral surface. The nodal coordinates of each point can be expressed as Equation (8).

$$e_i = \left[r_i \quad \frac{\partial r_i}{\partial X} \quad \frac{\partial r_i}{\partial Y} \right] \tag{8}$$

The first term in the expression represents the position coordinate array, while the second to the third terms represent the gradient coordinate array. Here, i represents the points A, B, C, and D, and the specific expressions for each term are as Equation (9).

$$\begin{cases} r_i = [r_{i,x} & r_{i,y} & r_{i,z}] \\ \frac{\partial r_i}{\partial X} = \left[\frac{\partial r_{i,x}}{\partial X} & \frac{\partial r_{i,y}}{\partial X} & \frac{\partial r_{i,z}}{\partial X} \right] \\ \frac{\partial r_i}{\partial Y} = \left[\frac{\partial r_{i,x}}{\partial Y} & \frac{\partial r_{i,y}}{\partial Y} & \frac{\partial r_{i,z}}{\partial Y} \right] \end{cases} \tag{9}$$

Therefore, the expression for the nodal coordinates of the element is as Equation (10).

$$e = [e_A \quad e_B \quad e_C \quad e_D] \tag{10}$$

The position vector of any point Q on the neutral surface of the shell element in the global coordinate system is given by Equation (11).

$$r^{\text{mid}} = S(\alpha, \beta)e \tag{11}$$

In the expression, S represents the shape function of the shell element. The expression for S is Equation (12).

$$S = [S_1I_3 \quad S_2I_3 \quad \cdots \quad S_{12}I_3] \tag{12}$$

In Equation (12), I₃ denotes the third-order identity matrix.

Therefore, the expressions for the velocity and acceleration of any point on the shell element can be obtained from the equation in Equation (13).

$$\dot{r}^{\text{mid}} = S(\alpha, \beta)\dot{e}, \quad \ddot{r}^{\text{mid}} = \dot{S}(\alpha, \beta)\dot{e} \tag{13}$$

2.2. Deformation Modeling of Shell Units

As shown in Figure 2b, the schematic diagram represents a surface within the shell element, with the global coordinate system denoted as X-Y-Z and the α-β-γ system representing the curvilinear coordinates on the surface of the shell element.

The $g_x^0 - g_y^0 - n^0$ and $e_x^0 - e_y^0 - n^0$ corresponds to the local curvilinear coordinate system and the Cartesian coordinate system on the shell element, respectively. Where the superscript (0) indicates before the deformation, and the subscript (x, y) is used to distinguish the axes.

The macro vector (dr_{mid}^0, dr_{mid}) and its corresponding micro arc length (ds^0, ds) between two adjacent points Q and P on the midplane before and after the deformation can be written as Equation (14).

$$\left\{ \begin{array}{l} dr_{mid}^0 = g_x^0 d\alpha + g_y^0 d\beta \\ dr_{mid} = g_x d\alpha + g_y d\beta \\ (ds^0)^2 = (dr_{mid}^0)^T \cdot dr_{mid}^0 = \begin{bmatrix} d\alpha & d\beta \end{bmatrix} \begin{bmatrix} (g_x^0)^T g_x^0 & (g_x^0)^T g_y^0 \\ (g_y^0)^T g_x^0 & (g_y^0)^T g_y^0 \end{bmatrix} \begin{bmatrix} d\alpha \\ d\beta \end{bmatrix} \\ (ds)^2 = (dr_{mid})^T \cdot dr_{mid} = \begin{bmatrix} d\alpha & d\beta \end{bmatrix} \begin{bmatrix} g_x^T g_x & g_x^T g_y \\ g_y^T g_x & g_y^T g_y \end{bmatrix} \begin{bmatrix} d\alpha \\ d\beta \end{bmatrix} \end{array} \right. \quad (14)$$

From Equation (14), the definition of the basis vectors for two sets of local coordinate systems on the mid-surface is as Equation (15).

$$\left\{ \begin{array}{l} g_x = \frac{\partial r_{mid}}{\partial \alpha}, g_y = \frac{\partial r_{mid}}{\partial \beta}, n = \frac{g_x \times g_y}{\|g_x \times g_y\|_2} \\ e_x = \frac{g_x}{\|g_x\|_2}, e_z = n, e_y = e_z \times e_x \end{array} \right. \quad (15)$$

Coordinate transformation yields can be expressed as Equation (16).

$$\begin{bmatrix} d\alpha \\ d\beta \end{bmatrix} = \begin{bmatrix} g_x e_x & g_y e_x \\ g_x e_y & g_y e_y \end{bmatrix}^{-T} \begin{bmatrix} dx_0 \\ dy_0 \end{bmatrix} = \begin{bmatrix} \frac{1}{a} & -\frac{\cot(\theta)}{a} \\ 0 & \frac{\csc(\theta)}{b} \end{bmatrix} \begin{bmatrix} dx_0 \\ dy_0 \end{bmatrix} = T_\theta dX_0 \quad (16)$$

Here, T_θ represents the transformation matrix from the Cartesian coordinate system to the curvilinear coordinate system, where θ denotes the angle between the coordinate axes of the curvilinear coordinate system.

From Equation (14), the formula for calculating the Lagrange strain tensor can be derived from continuum mechanics as Equation (17).

$$(ds)^2 - (ds_0)^2 = 2dX_0 \epsilon dX_0 \quad (17)$$

The expression for the mid-surface Lagrange strain tensor is obtained as Equation (18).

$$\epsilon_{mid} = \frac{1}{2} T_\theta^T \left(\begin{bmatrix} g_x^T g_x - (g_x^0)^T g_x^0 & g_x^T g_y - (g_x^0)^T g_y^0 \\ g_y^T g_x - (g_y^0)^T g_x^0 & g_y^T g_y - (g_y^0)^T g_y^0 \end{bmatrix} \right) T_\theta = \begin{bmatrix} \epsilon_{11} & \epsilon_{12} \\ \epsilon_{21} & \epsilon_{22} \end{bmatrix} \quad (18)$$

Since ϵ_{mid} has symmetry, ϵ_{mid} can be rewritten as Equation (19).

$$\epsilon_{mid} = [\epsilon_{11} \quad \epsilon_{22} \quad 2\epsilon_{12}]^T \quad (19)$$

From Figure 2a, the position vector of any point Q' on the external surface of the shell unit can be expressed as Equation (20).

$$r = r_{mid}(\alpha, \beta) + zn(\alpha, \beta) \quad (20)$$

Then, the basis vector of the surface coordinate system at point Q' can be calculated by Equation (21).

$$\begin{cases} \mathbf{g}'_x = \frac{\partial \mathbf{r}_{\text{mid}}(\alpha, \beta)}{\partial \alpha} + z \frac{\partial \mathbf{n}(\alpha, \beta)}{\partial \alpha} \\ \mathbf{g}'_y = \frac{\partial \mathbf{r}_{\text{mid}}(\alpha, \beta)}{\partial \beta} + z \frac{\partial \mathbf{n}(\alpha, \beta)}{\partial \beta} \end{cases} \quad (21)$$

Similarly, the length of the micro-segment arc between two adjacent points Q' and P' on the external surface before and after the deformation can be obtained by Equation (22).

$$\begin{cases} d(s'_0)^2 = [d\alpha \quad d\beta] \begin{bmatrix} (\mathbf{g}'_x)_0^T (\mathbf{g}'_x)_0 & (\mathbf{g}'_x)_0^T (\mathbf{g}'_y)_0 \\ (\mathbf{g}'_y)_0^T (\mathbf{g}'_x)_0 & (\mathbf{g}'_y)_0^T (\mathbf{g}'_y)_0 \end{bmatrix} \begin{bmatrix} d\alpha \\ d\beta \end{bmatrix} \\ d(s')^2 = [d\alpha \quad d\beta] \begin{bmatrix} (\mathbf{g}'_x)^T \mathbf{g}'_x & (\mathbf{g}'_x)^T \mathbf{g}'_y \\ (\mathbf{g}'_y)^T \mathbf{g}'_x & (\mathbf{g}'_y)^T \mathbf{g}'_y \end{bmatrix} \begin{bmatrix} d\alpha \\ d\beta \end{bmatrix} \end{cases} \quad (22)$$

The Lagrange strain tensor for the shell element can be calculated by Equation (23).

$$\boldsymbol{\varepsilon} \approx \boldsymbol{\varepsilon}_{\text{mid}} + \boldsymbol{\varepsilon}_b = \frac{1}{2} \mathbf{T}_\theta^T \begin{bmatrix} (\mathbf{g}'_x)^T \mathbf{g}'_x - (\mathbf{g}'_x)_0^T (\mathbf{g}'_x)_0 & (\mathbf{g}'_x)^T \mathbf{g}'_y - (\mathbf{g}'_x)_0^T (\mathbf{g}'_y)_0 \\ (\mathbf{g}'_y)^T \mathbf{g}'_x - (\mathbf{g}'_y)_0^T (\mathbf{g}'_x)_0 & (\mathbf{g}'_y)^T \mathbf{g}'_y - (\mathbf{g}'_y)_0^T (\mathbf{g}'_y)_0 \end{bmatrix} \mathbf{T}_\theta \quad (23)$$

where ε_b is unit bending strain.

By neglecting higher-order terms in z , we obtain Equations (24) and (25).

$$\boldsymbol{\varepsilon}_b = -z \mathbf{A}^T (\mathbf{l} - \mathbf{l}_0) \mathbf{A} \quad (24)$$

$$\begin{cases} \mathbf{l} = \begin{bmatrix} \left(\frac{\partial^2 \mathbf{r}_{\text{mid}}}{\partial \alpha^2} \right)^T \cdot \mathbf{n} & \left(\frac{\partial^2 \mathbf{r}_{\text{mid}}}{\partial \alpha \partial \beta} \right)^T \cdot \mathbf{n} \\ \left(\frac{\partial^2 \mathbf{r}_{\text{mid}}}{\partial \beta \partial \alpha} \right)^T \cdot \mathbf{n} & \left(\frac{\partial^2 \mathbf{r}_{\text{mid}}}{\partial \beta^2} \right)^T \cdot \mathbf{n} \end{bmatrix} = \begin{bmatrix} l_{11} & l_{12} \\ l_{12} & l_{22} \end{bmatrix} \\ \mathbf{l}_0 = \begin{bmatrix} \left(\frac{\partial^2 \mathbf{r}_{\text{mid}}^0}{\partial \alpha^2} \right)^T \cdot \mathbf{n} & \left(\frac{\partial^2 \mathbf{r}_{\text{mid}}^0}{\partial \alpha \partial \beta} \right)^T \cdot \mathbf{n} \\ \left(\frac{\partial^2 \mathbf{r}_{\text{mid}}^0}{\partial \beta \partial \alpha} \right)^T \cdot \mathbf{n} & \left(\frac{\partial^2 \mathbf{r}_{\text{mid}}^0}{\partial \beta^2} \right)^T \cdot \mathbf{n} \end{bmatrix} = \begin{bmatrix} l_{11}^0 & l_{12}^0 \\ l_{21}^0 & l_{22}^0 \end{bmatrix} \end{cases} \quad (25)$$

2.3. Flexible Interface Dynamics Model

Let the volume of the shell unit be V_e , and then the virtual work of the inertial force on the shell unit can be calculated by Equation (26).

$$\delta W_{ge} = - \int_{V_e} \rho \ddot{\mathbf{r}}^T \delta \mathbf{r} dV_e = - \ddot{\mathbf{e}}^T \left(\int_{V_e} \rho \mathbf{S}^T \mathbf{S} dV_e \right) \delta \mathbf{e} = - \ddot{\mathbf{e}}^T \mathbf{M}_e \delta \mathbf{e} \quad (26)$$

where $\mathbf{M}_e = \int_{V_e} \rho \mathbf{S}^T \mathbf{S} dV_e$ is the mass matrix of the shell unit.

Therefore, the virtual work of inertia force for the flexible interface can be calculated by Equation (27).

$$\delta W_{gd} = - \sum_{j=1}^n \int_{V_{ej}} \rho \ddot{\mathbf{r}}^T \delta \mathbf{r} dV_{ej} = - \ddot{\mathbf{q}}_f^T \mathbf{M}_f \delta \mathbf{q}_f \quad (27)$$

where n is the number of shell units after interface discretization; V_{ej} is the volume of the j -th shell unit.

\mathbf{q}_f is the generalized coordinates of the interface that can be calculated by Equation (28).

$$\mathbf{q}_f = [\mathbf{e}_1^T \cdots \mathbf{e}_i^T \cdots \mathbf{e}_n^T]^T, \quad \mathbf{M}_f = \sum_{j=1}^n \mathbf{B}_j^T \mathbf{M}_{ej} \mathbf{B}_j \quad (28)$$

where B_j is denoted as the boolean matrix corresponding to each shell cell.

As the deformation of the shell element is decomposed into the bending deformation of the shell element and the mid-surface deformation, the strain energy of the shell element can be decomposed into the bending strain energy (U_b) and the mid-surface deformation strain energy (U_{mid}), that can be calculated by the following formulas.

$$U_b = \frac{1}{2} \int_{V_e} (\boldsymbol{\varepsilon}_b)^T \mathbf{E} \boldsymbol{\varepsilon}_b dV_e = \frac{1}{2} \int_{V_e} \boldsymbol{\Phi}^T \mathbf{K}^T \mathbf{E} \mathbf{K} \boldsymbol{\Phi} dV_e \quad (29)$$

$$U_{mid} = \frac{1}{2} \int_{V_e} (\boldsymbol{\varepsilon}_{mid})^T \mathbf{E} \boldsymbol{\varepsilon}_{mid} dV_e \quad (30)$$

where \mathbf{E} is the third-order modulus of the elasticity matrix; \mathbf{K} is the equivalent transformation matrix of the bending strain tensor.

$$\mathbf{E} = \frac{E}{1-\nu^2} \begin{bmatrix} 1 & \nu & 0 \\ \nu & 1 & 0 \\ 0 & 0 & \frac{1-\nu}{2} \end{bmatrix}$$

$$\boldsymbol{\Phi} = -z [l_{11} - l_{11}^0 \quad l_{22} - l_{22}^0 \quad 2l_{12} - 2l_{12}^0]^T \quad (31)$$

$$\mathbf{K} = \begin{bmatrix} \frac{1}{a^2} & 0 & 0 \\ \frac{\cot^2(\theta)}{a^2} & \frac{\csc^2(\theta)}{b^2} & -\frac{\cot(\theta) \csc(\theta)}{ab} \\ -\frac{2 \cot(\theta)}{a^2} & 0 & \frac{\csc(\theta)}{ab} \end{bmatrix}$$

where ν is Poisson's ratio.

The derivative of the strain energy for the generalized coordinates yields the elastic forces on the neutral surface.

$$\mathbf{F}_{mid} = \frac{\partial U_{mid}}{\partial \mathbf{e}} = \int_{V_e} \left(\frac{\partial \boldsymbol{\varepsilon}_{mid}}{\partial \mathbf{e}^T} \right)^T \mathbf{E} \boldsymbol{\varepsilon}_{mid} dV_e \quad (32)$$

The bending strain energy is derived for the generalized coordinates to obtain the bending elastic force as Equation (33).

$$\mathbf{F}_b = \frac{\partial U_b}{\partial \mathbf{e}} = \int_{V_e} \left(\frac{\partial \boldsymbol{\varepsilon}_b}{\partial \mathbf{e}^T} \right)^T \mathbf{E} \boldsymbol{\varepsilon}_b dV_e = \int_{V_e} \left(\frac{\partial \boldsymbol{\Phi}}{\partial \mathbf{e}^T} \right)^T \mathbf{K}^T \mathbf{E} \mathbf{K} \boldsymbol{\Phi} dV_e \quad (33)$$

Then, the shell unit elastic force is $F_{se} = F_{mid} + F_b$, so the internal force virtual work of the shell unit is $\delta W_{ie} = F_{se}^T \delta \mathbf{e}$, and the internal force virtual work of the flexible interface can be calculated by Equations (34) and (35).

$$\delta W_{id} = \sum_{j=1}^n \mathbf{F}_{se}^T \delta \mathbf{e} = -\mathbf{Q}_s^T \delta \mathbf{q}_f \quad (34)$$

$$\mathbf{Q}_s = \sum_{i=1}^n \mathbf{F}_e \mathbf{B}_i \quad (35)$$

Let the generalized force acting on the interface be \mathbf{Q}_a , and then its corresponding external virtual work can be calculated by Equation (36).

$$\delta W_{ed} = \mathbf{Q}_a^T \delta \mathbf{q}_f \quad (36)$$

Then, from the principle of virtual work, we can obtain the equation as Equation (37).

$$\begin{aligned}\delta W_{gd} + \delta W_{id} + \delta W_{ed} &= -\ddot{q}_f^T M_g \delta q_f - Q_s^T \delta q_f + Q_a^T \delta q_f \\ &= (M_f \ddot{q}_f - Q_f)^T \delta q_f = 0\end{aligned}\quad (37)$$

where $Q_f = Q_a - Q_s$.

Then, the kinetic equation of the flexible interface without external constraints can be expressed as Equation (36).

$$M_f \ddot{q}_f - Q_f = 0 \quad (38)$$

2.4. Dynamics Model of the Mast Deployment Process with Replaceable Interface

The schematic diagram of the interchangeable interface mast system, known as the “three interfaces and four modules”, is illustrated in Figure 3.

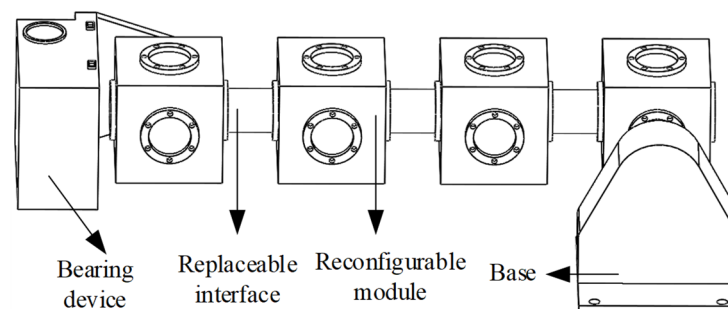


Figure 3. Schematic diagram of replaceable interface mast composition.

When deriving the dynamics equations for the expansion process of the interchangeable interface mast system, the following assumptions are made:

- (1) The reconfigurable module is considered a rigid joint between the reconfigurable module and the flexible interface;
- (2) The rotation constraint is between the reconfigurable module and the body of the rover (base);
- (3) The mast deployment process does not consider the effect of gravity;
- (4) The body of the rover is considered a rigid body, and the body of the rover is at rest when the mast is deployed.

After establishing the dynamic equations for each part separately, it is necessary to establish the dynamic equations of the mast system by simultaneously combining the dynamic models of each part via the system’s constraint equations. The constraints of the mast system include the articulated constraints between the reconfigurable modules and the inspector body, the rigid joints between the reconfigurable modules and the flexible interfaces, as well as the intrinsic constraints introduced when modeling the reconfigurable modules using NCF (Natural Coordinate Formulation) [27].

The reconfigurable modules, which are described by the NCF method to depict the motion of rigid bodies, possess 12 generalized coordinates. Consequently, it is necessary to impose six constraints, including the mutual orthogonality constraints between three basis vectors and the length constraints of the basis vectors. The expression for the constraint equations of the rigid body is Equation (39).

$$\Phi_{q_r} : \begin{cases} \|r_j - r_i\| = d, & u^T (r_j - r_i) = 0 \\ \|u\| = 1, & v^T (r_j - r_i) = 0 \\ \|v\| = 1, & u^T v = 0 \end{cases} \quad (39)$$

where d is the side length of the reconstructed module (m).

2.5. Fixed Constraints

The rigid joint limits the position between the origin of the coordinate system on the shell unit and the nodes on the rigid module and the rotation of the interchangeable interface for the rigid module, as shown in Figure 4.

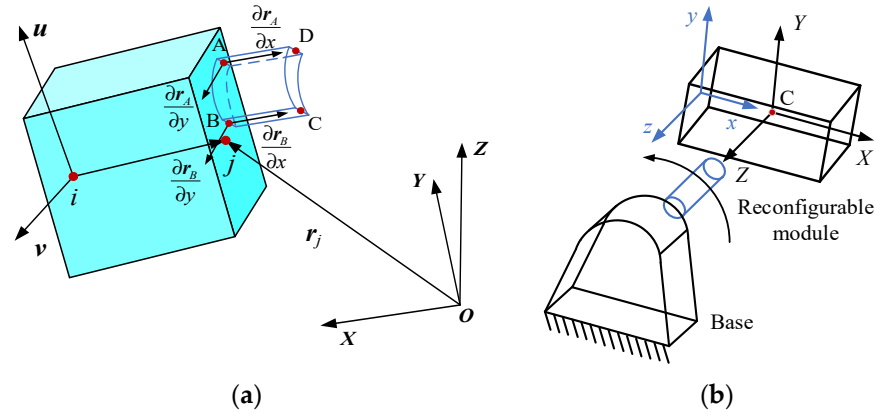


Figure 4. Schematic diagram of rigid joint (a) and rotational constraints (b).

The gradient vector along the x-direction at the nodes A and B during the unfolding process is always perpendicular to the vector u and v . As Equation (40).

$$\Phi_f : \begin{cases} \|r_A - r_j\|_2 = \|\bar{r}_{Aj}\|_2 \\ \|r_B - r_j\|_2 = \|\bar{r}_{Bj}\|_2 \\ \frac{\partial r_A}{\partial x} \cdot u = 0 \\ \frac{\partial r_B}{\partial x} \cdot u = 0 \\ \frac{\partial r_A}{\partial x} \cdot v = 0 \\ \frac{\partial r_B}{\partial x} \cdot v = 0 \end{cases} \quad (40)$$

where $\|\bar{r}_{Aj}\|_2, \|\bar{r}_{Bj}\|_2$ is the radius of the neutral surface of the interface.

2.6. Rotation Constraints

The revolute joints between the reconfigurable module and the base are illustrated in Figure 4b. Here, the x - y - z axes represent the local coordinate system of the rigid body, while the X - Y - Z axes represent the global coordinate system. Thus, the center of mass of the rigid body module coincides with the origin of the global coordinate system. Additionally, during the rotation of the rigid body module, the ox and oy axes are always perpendicular to the Oz axis. Hence, the constraint equations can be expressed as Equation (41).

$$\Phi_R : \begin{cases} r_c = 0 \\ \begin{bmatrix} 0 & 0 & 1 \end{bmatrix} \cdot u = 0 \\ \begin{bmatrix} 0 & 0 & 1 \end{bmatrix} \cdot r_{ji} = 0 \end{cases} \quad (41)$$

2.7. Mast System Dynamics Equation

For a system of replaceable interface masts with m flexible interfaces and n reconfigurable modules, the dynamical equations in the unfolding process can be expressed as Equation (41).

$$-\sum_{i=1}^n \delta q_{ri}^T (M_{ri} \ddot{q}_{ri} - Q_{ri}) + \sum_{j=1}^m \delta q_{fj}^T (M_{fj} \ddot{q}_{fj} - Q_{fj}) = 0 \quad (42)$$

Let $q = [q_{r1} \cdots q_{rn} q_{f1} \cdots q_{fm}]^T$ be the generalized coordinates of the total interchangeable interface mast system, then the above equation can be rewritten as Equation (43).

$$-\delta q^T (M\ddot{q} - Q_a) = 0 \tag{43}$$

$$M = \text{diag}\{M_{r1} \cdots M_{rn} M_{f1} \cdots M_{fm}\}, Q_a = [Q_{r1} \cdots Q_{rn} Q_{f1} \cdots Q_{fm}]$$

The replaceable interface mast system has a total of 1 revolute joint and $2m$ rigid joints, and the constraint equation of the mast system can be obtained by Equation (44).

$$\Phi(q_r, q_d, t) = 0 \tag{44}$$

where $q_d = [q_{f1} q_{f2} \cdots q_{fm}]$ is the total generalized coordinate of the interface contained in the mast system.

For the simplified model under ideal conditions, the damping term is excluded in order to reduce the computational complexity and quickly obtain the approximate solution. The dynamical equations in matrix form during the unfolding of the mast system can be obtained by associating the Lagrange multiplier method. As Equation (45).

$$\begin{bmatrix} M & \Phi_q^T \\ \Phi_q & 0 \end{bmatrix} \begin{bmatrix} \ddot{q} \\ \lambda \end{bmatrix} = \begin{bmatrix} Q_a \\ \psi \end{bmatrix} \tag{45}$$

where Φ_q is the Jacobi matrix of the system constraint equations for the generalized coordinates of the system; λ is the Lagrange multiplier array.

By taking the second derivative of time of the constraint equation $\Phi(q_r, q_d, t)$ and organizing the equation, the expression of ψ is obtained as Equation (46).

$$\begin{aligned} \psi = \Phi_q \ddot{q} = & -(\Phi_{q_r} \dot{q}_r)_{q_r} \dot{q}_r - (\Phi_{q_r} \dot{q}_r)_{q_d} \dot{q}_f - (\Phi_{q_f} \dot{q}_d)_{q_d} \dot{q}_d \\ & - (\Phi_{q_d} \dot{q}_d)_{q_r} \dot{q}_r - 2(\Phi_{q_r t} \dot{q}_r + \Phi_{q_d t} \dot{q}_d) - \Phi_{tt} \end{aligned} \tag{46}$$

3. Analysis of the Effect of Nonlinear Parameters on Mast Deployment

To provide a reference for the actual design and structural configuration of the replaceable mast, it is necessary to analyze the mast dynamic behavior in-depth under different configurations of structural solutions, interface radius of curvature, section thickness, and driving law factors. The schematic of the comparative analysis of mast system parameters is shown in Figure 5.

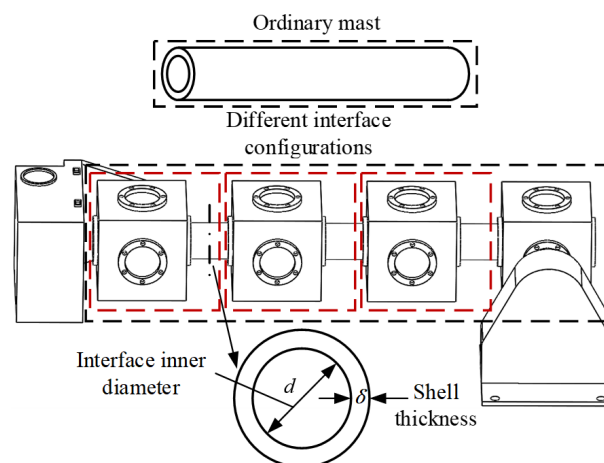


Figure 5. The schematic diagram of the comparative analysis of mast system parameters.

The trapezoidal velocity plan is chosen for unfolding the drive method of the joint due to its widely used, and the joint angular velocity equation can be expressed as Equation (47).

$$\omega = \begin{cases} 150t & , 0 \leq t \leq 0.1 \\ 15 & , 0.1 \leq t \leq 6 \\ -150t + 915 & , 6 \leq t \leq 6.1 \\ 0 & , 6.1 \leq t \end{cases} \quad (47)$$

3.1. Non-Linear Effects of Structural Configuration

Table 1 shows the basic geometric parameters of the relevant components of the replaceable mast system, and Table 2 shows the material parameters of the components of the replaceable mast system.

Table 1. Basic geometric parameters of the replaceable mast system.

Parameter Name	Parameter Value/mm
Replaceable interface lengths	105
Replaceable interface inner diameter	84
Replaceable interface thickness	2
Reconfigurable module edge length	200

Table 2. Material parameters of the replaceable mast system.

Parameter Name	Parameter Value
Modulus of elasticity of replaceable interface/Pa	2.4×10^9
Replaceable interface Poisson’s ratio	0.35
Replaceable interface density/Kg · m ⁻³	1100
Modulus of reconfigurable module/Pa	2×10^{11}
Reconfigurable density/Kg · m ⁻³	7850

Based on the above settings, we used the numerical software ADAMS to model and simulate the system dynamics model, which consisted of the rigid body module that acts as the deployment joint and the flexible interface connected to it. The x and y displacement of the mast at its endpoints is shown in Figure 6a,b when the mast is deployed in the x and y directions with the ADAMS simulation results.

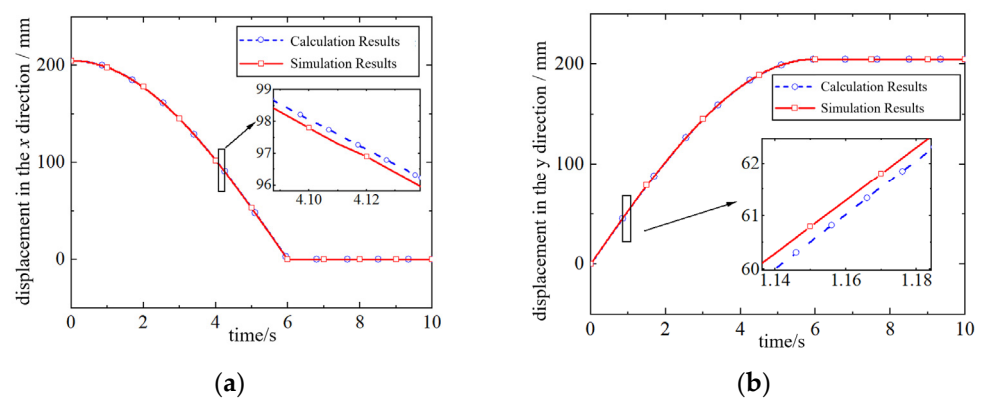


Figure 6. Comparison of the calculation and simulation results of the displacement (a) in the x-direction and (b) in the y-direction.

The calculated results of the linear velocity in the x and y direction of the endpoint of the mast are compared with the ADAMS simulation results, as shown in Figure 7a,b.

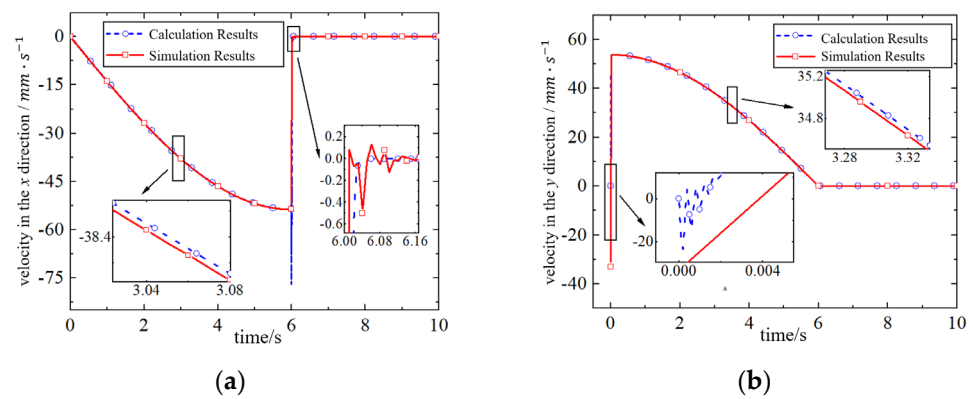


Figure 7. Comparison of the calculation and simulation results of the velocity (a) in the x-direction and (b) in the y-direction.

In general, the x and y displacement and linear velocity curves of the theoretical model are basically consistent with the simulation curves, which can verify the correctness of the dynamic model of the replaceable interface mast system.

The three-mast combination schemes are shown in Figure 8. Scheme 1 is assembled by one flexible interface in series with two reconfigurable rigid modules. Scheme 2 uses two replaceable interfaces to connect three reconfigurable modules. Scheme 3 is assembled by three replaceable interfaces and four reconfigurable modules.

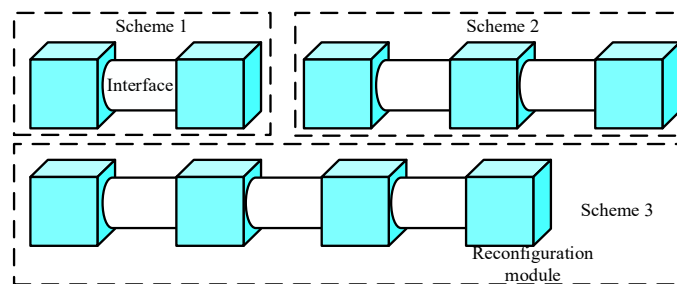


Figure 8. Schematic diagram of the structure of different combination schemes.

The comparison of the angular acceleration at the end of the mast and the force at the deployment joint for different scenarios is shown in Figures 9 and 10, where scheme 3 has a large mass moment of inertia. Therefore, under the same velocity plan, the force at the deployment joint is the largest and the acceleration generated at the end is also the largest and lasts the longest.

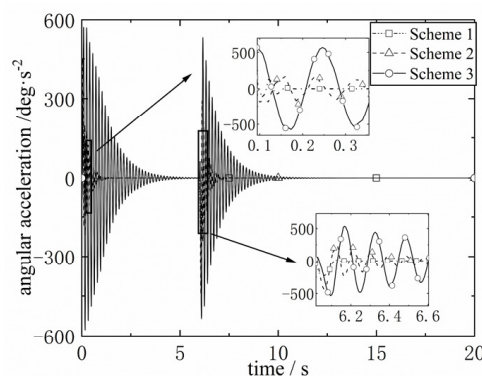


Figure 9. Absolute angular acceleration.

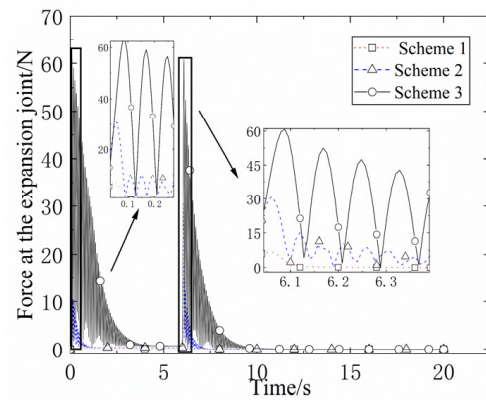


Figure 10. Force at the expansion joint.

3.2. Non-Linear Effect of Different Shell Thickness and Diameter

The mast model is selected as the replaceable interface mast in scheme 3, and the interface shell thickness is set as $\delta = 0.5$ mm, $\delta = 1.0$ mm, and $\delta = 1.5$ mm for three cases. The angular acceleration and the force at the unfolded joint for the three shell thicknesses are shown in Figures 11 and 12.

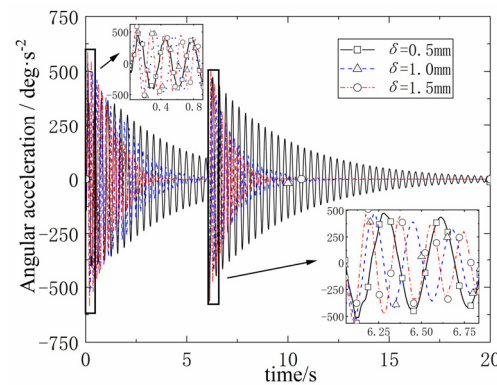


Figure 11. Absolute angular acceleration.

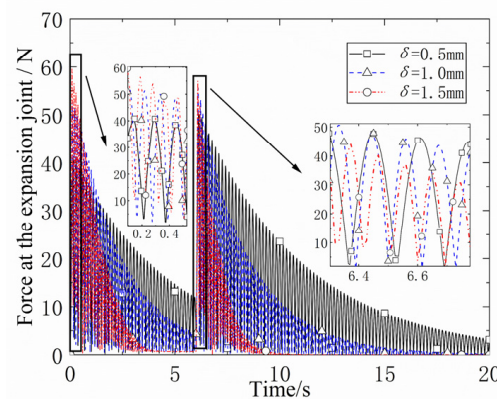


Figure 12. Expanding joint forces.

Based on comparative analysis, it was observed that the attenuation of angular acceleration during the mast alignment process and residual vibration process is directly proportional to the shell thickness. As the shell thickness increases, the force at the deployment joint attenuates more rapidly, resulting in a shorter duration of angular acceleration vibrations.

The same configuration is carried out according to scheme 3, and the inner diameter of the interface is set as $d = 85$ mm, $d = 90$ mm, and $d = 100$ mm.

The absolute angular acceleration at the end of the mast and the change of force at the deployment joint are shown in Figures 13 and 14. The results show that the interface in the replaceable mast should be designed with the system requirements in mind while appropriately expanding the inner diameter of the interface to improve the vibration and deformation resistance of the mast system.

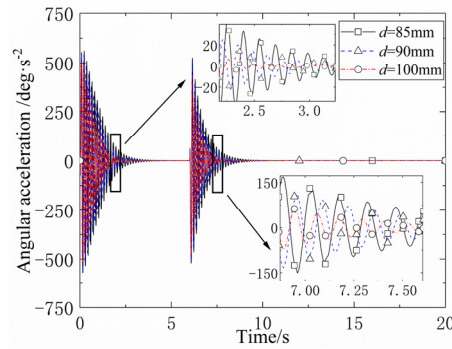


Figure 13. Absolute angular acceleration.

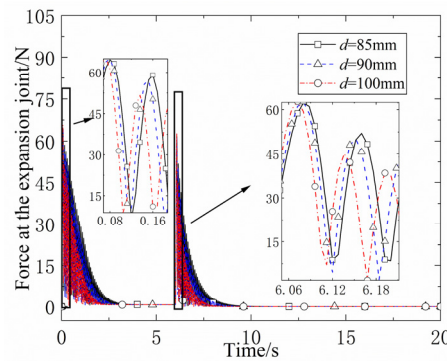


Figure 14. Force at the spread joint.

3.3. Driving Law Non-Linear Influence

The unfolded joint angles are planned for cubic polynomial, quintuple polynomial, and pendulum motion laws. The initial conditions of motion are given as Equation (48).

$$\begin{cases} \theta_c(0) = 0, \dot{\theta}_c(0) = 0 \\ \theta_c(t_c) = \frac{\pi}{2}, \dot{\theta}_c(t_c) = 0 \end{cases}, \begin{cases} \theta_q(0) = 0, \theta_q(t_q) = \pi/2 \\ \dot{\theta}_q(0) = 0, \dot{\theta}_q(t_q) = 0 \\ \ddot{\theta}_q(0) = 0, \ddot{\theta}_q(t_q) = 0 \end{cases} \quad (48)$$

Then, the corresponding joint angle cubic and quintuple polynomial planning can be expressed as Equation (49).

$$\begin{aligned} \theta_c(t) &= \frac{\pi}{2} - \pi \left(\frac{t}{t_c}\right)^3 + \frac{3\pi}{2} \left(\frac{t}{t_c}\right)^2 \\ \theta_q &= 3\pi \left(\frac{t}{t_q}\right)^5 - \frac{15\pi}{2} \left(\frac{t}{t_q}\right)^4 + 5\pi \left(\frac{t}{t_q}\right)^3 \end{aligned} \quad (49)$$

The equation for the law of motion of the joint angle pendulum [9] can be expressed as Equation (50).

$$\theta_b(t) = \frac{\pi}{2} \left[\frac{t}{t_b} - \frac{1}{2\pi} \sin\left(\frac{2\pi t}{t_b}\right) \right] \quad (50)$$

The absolute and relative angular accelerations at the endpoint of the mast under the three types of motion are shown in Figures 15 and 16. The mast with the unfolding joint

angle changing according to the cubic polynomial has the worst stability and the most violent vibration, and the sudden change in acceleration at the beginning and the end of the motion causes a large vibration in the angular acceleration with amplitudes of 23.24 deg/s^2 and 24.10 deg/s^2 , respectively. The decay time of the angular acceleration is the longest under the law of motion.

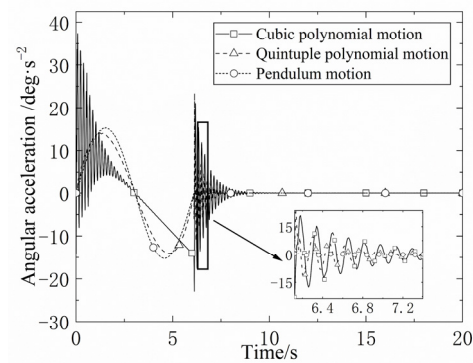


Figure 15. Absolute angular acceleration.

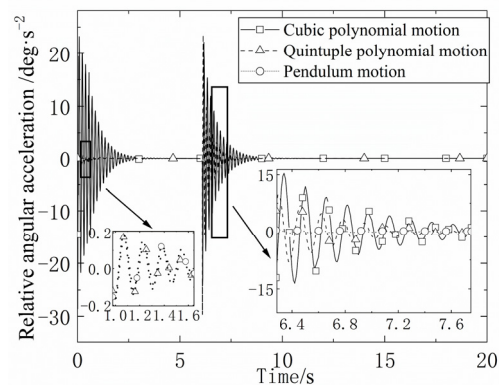


Figure 16. Relative angular acceleration.

3.4. Experimental Analysis of Replaceable Mast Deployment

When performing ground deployment experiments with replaceable masts, ground gravity will directly affect the experimental results, so the effect of gravity needs to be compensated. In the replaceable interface mast deployment test, the position of the mast end in the vertical plane changes with time; in this case, the ordinary suspension method is difficult to meet the needs of gravity compensation, and at the same time, it is limited by the experimental conditions and the advanced follow-up active control suspension method cannot be adopted, so this study converts the motion of the mast in the vertical plane into the horizontal plane to avoid the position change of the mast endpoint along the vertical direction by fully considering the characteristics of the mast deployment motion, and at the same time, the roller is introduced into the system to change the sliding friction to rolling friction, which compensates for the influence of gravity to the greatest extent. A triaxial accelerometer is mounted at the center point of the mast end of the interchangeable interface. The experimental analysis of the unfolding process of the mast under different scheme configurations was carried out with a driving speed of 15 deg/s and a movement angle of 90 deg for the unfolding joints.

The mast deployment experimental system and the schematic diagram of the gravity compensation scheme are shown in Figures 17 and 18.

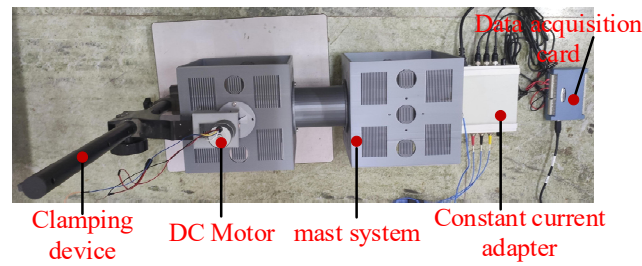


Figure 17. Mast deployment experimental system (Photographer: Jianmin Wen).



Figure 18. Schematic diagram of the gravity compensation scheme (Photographer: Jianmin Wen).

The acceleration comparison results of the endpoints of the mast under different scheme configurations are shown in Figure 19a–c.

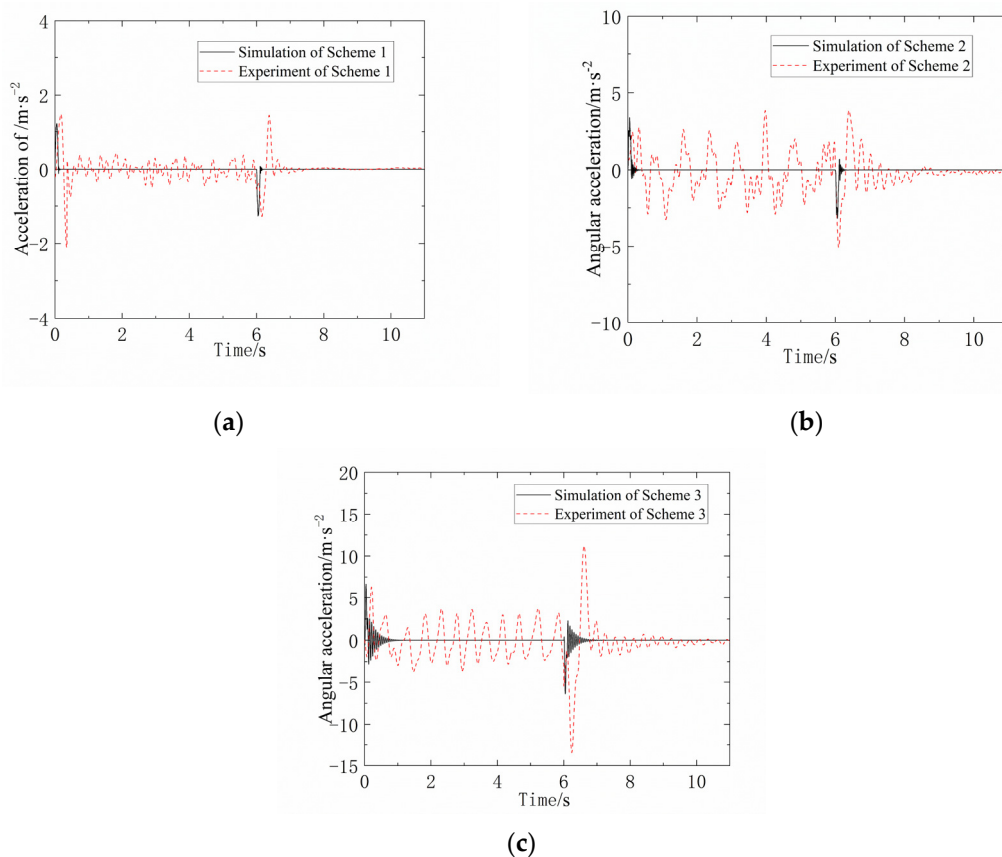


Figure 19. Comparison of Experiment and Simulation of scheme 1 (a), scheme 2 (b), scheme 3 (c).

The reconfigurable module used in the experiments is machined from resin material, so the simulation results need to be compared with those of interchangeable interface masts of the same material. At the same time, the triaxial acceleration sensor measures the linear acceleration along the tangential direction of the mast endpoint, while the simulation measures the angular acceleration signal at the mast endpoint. Therefore, the angular

acceleration signal obtained from the simulation is first converted into linear acceleration and then compared with the experimental results.

The comparative analysis of experimental data has confirmed that the greater the number of interface configurations, the more pronounced the vibration of the mast system, as indicated by simulation results. Furthermore, during the abrupt change in motion state at the onset of movement, there was a high degree of conformity between the experimental and theoretical acceleration curves for all three scenarios, with similar acceleration oscillation amplitudes. Throughout the uniform deployment motion of the mast, the experimental acceleration curve consistently exhibited a certain degree of oscillation. Upon completion of the motion, the experimental curve took some time to stabilize compared to the theoretical results. This is primarily attributable to the incomplete compensation for the effects of gravity during the experimental process. Additionally, the inherent vibration of mechanical equipment such as motors and platforms, as well as the deformation of the reconfigurable module, also contributed to some extent to the observed discrepancies in the experimental results.

To verify the errors caused by the deformation of reconfigurable modules in the experiment, the flexible interface in scheme 1 is now replaced by a functional prototype with a more rigid interface for analysis. A comparison of the end acceleration of scheme 1 before and after the replacement of the interface function prototype is shown in Figure 20.

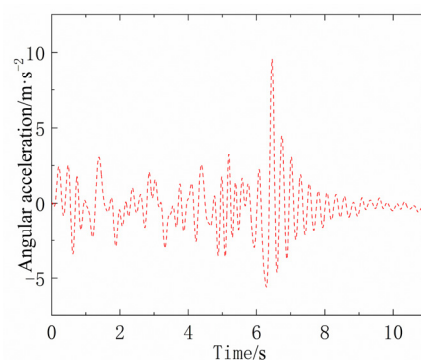


Figure 20. Acceleration before and after interface prototype replacement.

There are large vibrations in the acceleration during the entire unfolding of the mast. This is due to the flexible deformation of the reconfigurable module machined in the experiment leading to more intense vibration of the mast system.

4. Conclusions

In light of the limited redundancy and poor maintainability of conventional inspection mast systems, this paper combines the concepts of modular spacecraft and on-orbit replacement to propose the design concept of a redundant replaceable interface mast. Addressing the issue of system vibration caused by interface flexibility and its impact on the performance and operational quality of equipment mounted on the mast, the paper systematically investigates the deployment behavior and vibration suppression of a rigid-flexible coupled mast system. The research contributes valuable insights into the structural design, configuration planning, drive planning, and vibration control of replaceable interface masts.

The key achievements of this study include the following aspects:

- (1) Establishment of a dynamic model for the deployment process of the replaceable interface mast system. Considering the characteristics of the rigid-flexible multibody system of the replaceable interface mast, the paper models two types of components in the system separately and establishes the dynamic model of the mast system by incorporating system constraint equations. The comparison of numerical simulation results of the mast system's dynamic equations with software calculations demonstrates the correctness and effectiveness of the rigid-flexible multibody mast system's

dynamic model. This model holds significance for the dynamic modeling of complex systems involving multiple rigid and flexible bodies.

- (2) Analysis of the dynamic behavior changes during the deployment process of the replaceable mast system, investigating the influence of different system configuration schemes, interface geometric parameters, and various deployment motion patterns on the mast system's deployment behavior. Despite the higher mass of the replaceable interface mast compared to a regular mast of the same length, the introduction of a high-stiffness reconfigurable module in the replaceable mast increases the overall stiffness, resulting in reduced vibration deformation at the mast's endpoint. The quantity of flexible interfaces and reconfigurable rigid body modules in the mast system directly correlates with more drastic force variations at the deployment joint and nonlinear amplification of endpoint vibrations. Thinner interface shell thickness weakens the resistance to deformation, leading to increased endpoint vibrations and slower attenuation rates. Enlarging the interface's inner diameter increases the sectional moment of inertia, enhancing interface stiffness and accelerating the force attenuation at the deployment joint, resulting in decreased endpoint vibration. The use of harmonic motion planning minimizes mast vibration, underscoring the need to avoid sudden changes in angular acceleration and ensure a smooth acceleration profile to minimize vibrations. The theoretical model established considers and analyzes various nonlinear factors affecting the deployment behavior of the replaceable mast system, providing guidance for configuration, structural design, and drive planning of the mast.
- (3) Conducted on-ground deployment experiments for the replaceable interface mast, validating the scientific validity of the dynamic theoretical model and the correctness of simulation results. At the moment of abrupt change in the motion state at the beginning of the motion, the acceleration curves calculated by the experiment and the theory under the three schemes are in good agreement. The acceleration vibration amplitude is similar, while the experimental acceleration curve has a certain degree of vibration during the uniform motion of the mast. After the movement, it takes a period of time for the experimental curve to reach stability compared with the theoretical results. This is mainly because the influence of gravity cannot be completely offset during the experiment, and the jitter of the mechanical equipment, such as motors and platforms, and the deformation of reconfigurable modules will also have a certain impact on the experimental results. After the replacement of the interface prototype, there was a large vibration in the acceleration throughout the deployment of the mast. This is because there is a flexible deformation of the reconfigurable module processed in the experiment, and after replacing the flexible interface with a physical prototype of the interface with great stiffness, it is equivalent to increasing the load at the end of the reconfigurable module at the unfolded joint, which increases the generalized force array and the deformation of the reconfigurable module, so that the vibration of the mast system is more intense, which indicates that the elastic deformation of the reconfigurable module is indeed one of the sources of experimental error. Generally, Experimental results for different configuration schemes of the replaceable mast indicate that increasing the number of interfaces and reconfigurable modules intensifies mast vibrations.

While this paper presents significant contributions, areas for improvement have been identified for future research:

- (1) In the establishment of the mast system's dynamic model, further research can be conducted to examine the variations in mast system deployment behavior when considering the flexibility of reconfigurable modules.
- (2) The experiment lacks the analysis of the stability of the controller, which can be considered in the follow-up research to provide a reference for the optimal design.

- (3) Due to limitations in measurement equipment, the experiments verified only the acceleration of the mast's endpoint. Future research could extend the verification to include angular velocity at the endpoint and the torque at the deployment joint.

Author Contributions: T.L. conducted data extraction, performed the analyses, and wrote the article. J.W. conceived and designed the study, and applied for the funding which financially supported the study. Many of the figures were drawn by P.Z. and a special word of thanks goes to P.Z. for his efforts in checking the references. All authors have read and agreed to the published version of the manuscript.

Funding: This work is supported by the National Natural Science Foundation of China under Grant No. 52075116.

Data Availability Statement: The raw data supporting the conclusions of this article will be made available by the authors on request.

Conflicts of Interest: The authors declare that they have no known competing financial interests or personal relationships that could have appeared to influence the work reported in this paper.

References

- Warner, N.; Silverman, M.; Samuels, J.; DeFlores, L.; Sengstacken, A.; Maki, J.; Scodary, A.; Peters, S.; Litwin, T.; Metz, B. The Mars Science Laboratory Remote Sensing Mast. In Proceedings of the 2016 IEEE Aerospace Conference, Big Sky, MT, USA, 5–12 March 2016.
- Ren, J.; Kong, N.; Zhuang, Y.; Zhang, J.; Ma, S.; Wang, B.; Liu, W. A review on the interfaces of orbital replacement unit: Great efforts for modular spacecraft. *Proc. Inst. Mech. Eng. J. Aerosp. Eng.* **2021**, *235*, 1941–1967. [\[CrossRef\]](#)
- Rossetti, D.; Keer, B.; Panek, J.; Ritter, B.; Reed, B.B.; Cepollina, F. Spacecraft modularity for serviceable satellites. In Proceedings of the AIAA SPACE 2015 Conference and Exposition, Dallas, TX, USA, 22–26 June 2015.
- The Rover's "Neck and Head" [EB/OL]. Available online: <https://mars.nasa.gov/mer/mission/rover/neck-and-head/> (accessed on 27 May 2022).
- Mars Curiosity: Facts and Information [EB/OL]. Available online: <https://www.space.com/17963-mars-curiosity.html> (accessed on 27 May 2022).
- China's Change-3 Lander and Jade Rabbit Rover Land on Moon—SlashGear [EB/OL]. Available online: <https://www.slashgear.com/chinas-change-3-lander-and-jade-rabbitrover-land-on-moon-14308846/> (accessed on 27 May 2022).
- Zhang, C.; Yao, J.; Liu, Z.; Ding, L.; Cheng, F.; Qiu, H. Technological development of docking mechanism of manned spacecraft in China. *Spacecr. Eng.* **2022**, *31*, 205–212.
- Sun, P.; Xie, Z.; Gao, B.; Wu, G. Dynamic analysis of an on-orbit space docking mechanism. *Mech. Eng. Autom.* **2019**, *2*, 30–32.
- Wei, Q.; Wang, Y.; Tang, Z.; Zhang, D. Dynamic analysis of docking dynamics of auxiliary module of flexible manipulator arm of space station. *China Space Sci. Technol.* **2016**, *36*, 24–31. [\[CrossRef\]](#)
- Li, H.J.; Gao, H.B.; Deng, Z.Q. Design and analysis of the lunar rover mast mechanism. *Robot* **2008**, *30*, 13–16.
- Liu, G.; Liu, Y.; Zhang, H.; Gao, X.; Yuan, J.; Zheng, W. The kapvik robotic mast: An innovative onboard robotic arm for planetary exploration rovers. *IEEE Robot. Autom. Mag.* **2015**, *22*, 34–44.
- Hao, P.; You, B.; Sun, Y.; Liang, D. Nonlinear dynamic analysis of deployment of laminated planetary rover mast. In Proceedings of the 2017 IEEE International Conference on Cybernetics and Intelligent Systems (CIS) and IEEE Conference on Robotics, Automation and Mechatronics (RAM), Ningbo, China, 19–21 November 2017; IEEE: Piscataway, NJ, USA, 2017.
- Jonker, B. A Finite Element Dynamic Analysis of Flexible Manipulators. *Int. J. Robot. Res.* **1990**, *9*, 59–74. [\[CrossRef\]](#)
- Modi, V.J.; Mah, H.W.; Misra, A.K. On the non-linear dynamics of a space platform based mobile flexible manipulator. *Acta Astronaut.* **1994**, *32*, 419–439. [\[CrossRef\]](#)
- Li, Q.; Deng, Z.; Zhang, K.; Huang, H. Unified modeling method for large space structures using absolute nodal coordinate. *AIAA J.* **2018**, *56*, 4146–4157. [\[CrossRef\]](#)
- Nanos, K.; Papadopoulos, E.G. On the dynamics and control of flexible joint space manipulators. *Control. Eng. Pract.* **2015**, *45*, 230–243. [\[CrossRef\]](#)
- Meng, D.; She, Y.; Xu, W.; Lu, W.; Liang, B. Dynamic modeling and vibration characteristics analysis of flexible-link and flexible-joint space manipulator. *Multibody Syst. Dyn.* **2018**, *43*, 321–347. [\[CrossRef\]](#)
- Shabana, A.A. Flexible multibody dynamics: Review of past and recent developments. *Multibody Syst. Dyn.* **1997**, *1*, 189–222. [\[CrossRef\]](#)
- Dmitrochenko, O.N.; Pogorelov, D.Y. Generalization of plate finite elements for absolute nodal coordinate formulation. *Multibody Syst. Dyn.* **2003**, *10*, 17–43. [\[CrossRef\]](#)
- Sugiyama, H.; Koyama, H.; Yamashita, H. Gradient deficient curved beam element using the absolute nodal coordinate formulation. *J. Comput. Nonlinear Dyn.* **2010**, *5*, 021001. [\[CrossRef\]](#)

21. Liu, C.; Tian, Q.; Hu, H. New spatial curved beam and cylindrical shell elements of gradient-deficient Absolute Nodal Coordinate Formulation. *Nonlinear Dyn.* **2012**, *70*, 1903–1918. [[CrossRef](#)]
22. Vanpaemel, S.; Asrih, K.; Vermaut, M.; Naets, F. Topology optimization for dynamic flexible multibody systems using the Flexible Natural Coordinates Formulation. *Mech. Mach. Theory* **2023**, *185*, 105344. [[CrossRef](#)]
23. Vanpaemel, S.; Vermaut, M.; Desmet, W.; Naets, F. Input optimization for flexible multibody systems using the adjoint variable method and the flexible natural coordinates formulation. *Multibody Syst. Dyn.* **2023**, *57*, 259–277. [[CrossRef](#)]
24. Wang, T. Model Establishment and Motion Deformation Analysis of Flexible Plate Based on Absolute Nodal Coordinate Method. Ph.D. Thesis, Shijiazhuang Tiedao University, Shijiazhuang, China, 2023. [[CrossRef](#)]
25. Peng, Q.; Li, B.; Rong, K.; Qiao, Z.; Wang, S. Dynamic analysis of spreadable mechanism of scissor element using absolute nodal coordinate method. *J. Xi'an Jiaotong Univ.* **2023**, *57*, 172–181.
26. Zhang, H.; Xia, H.; Li, D.; Liu, J. Analysis of dynamic characteristics of three-dimensional flexible rotating beam based on absolute nodal coordinate method. *J. Guangdong Univ. Technol.* **2022**, *39*, 76–83.
27. Garcia-Vallejo, D.; Escalona, J.L.; Mayo, J.; Domínguez, J. Describing Rigid-Flexible Multibody Systems Using Absolute Coordinates. *Nonlinear Dyn.* **2003**, *34*, 75–94. [[CrossRef](#)]
28. Shabana, A.A. ANCF reference node for multibody system analysis. *Proc. Inst. Mech. Eng. J. Multi-Body Dyn.* **2014**, *229*, 109–112. [[CrossRef](#)]
29. Wang, Z.; Tian, Q.; Hu, H. Dynamics of spatial rigid-flexible multibody systems with uncertain interval parameters. *Nonlinear Dyn.* **2016**, *84*, 527–548. [[CrossRef](#)]
30. Li, K.; Tian, Q.; Shi, J.; Liu, D. Assembly dynamics of a large space modular satellite antenna. *Mech. Mach. Theory* **2019**, *142*, 103601. [[CrossRef](#)]
31. Li, Y.; Wang, C.; Huang, W. Dynamics analysis of planar rigid-flexible coupling deployable solar array system with multiple revolute clearance joints. *Mech. Syst. Signal Process.* **2019**, *117*, 188–209. [[CrossRef](#)]

Disclaimer/Publisher's Note: The statements, opinions and data contained in all publications are solely those of the individual author(s) and contributor(s) and not of MDPI and/or the editor(s). MDPI and/or the editor(s) disclaim responsibility for any injury to people or property resulting from any ideas, methods, instructions or products referred to in the content.